# IMPEDANCE STUDIES OF 2D AZIMUTHALLY SYMMETRIC DEVICES OF FINITE LENGTH

N. Biancacci (CERN, Geneva; Rome University "La Sapienza", Rome),
V.G.Vaccaro (CERN, Geneva; University Federico II, Naples)
E.Métral, B.Salvant (CERN, Geneva),
M.Migliorati, L.Palumbo (Rome University "La Sapienza", Rome)

*Abstract*

In circular accelerators, the beam quality can be strongly affected by the self-induced electromagnetic fields excited by the beam in the passage through the elements of the accelerator. The beam coupling impedance quantifies this interaction and allows predicting the stability of the dynamics of high intensity, high brilliance beams. The coupling impedance can be evaluated with finite element methods or using analytical methods, such as Field Matching or Mode Matching. In this paper we present an application of the Mode Matching technique for an azimuthally uniform structure of finite length: a cylindrical cavity loaded with a toroidal slab of lossy dielectric, connected with cylindrical beam pipes. In order to take into account the finite length of the structure, with respect to the infinite length approximation, we decompose the fields in the cavity into a set of orthonormal modes. We obtain a complete set of equations using the magnetic field matching and the non-uniform convergence of the electric field on the cavity boundaries. We present benchmarks done with CST Particle Studio simulations and existing analytical formulas, pointing out the effect of finite length and non-relativistic beta.

## INTRODUCTION

The problem of calculating the impedance of finite length devices, in particular simple cavities, has been approached in different ways: it was studied as a field matching problem in [1], and, approximated as a thin insert in [2, 3].

In this application we want to study rigorously the electromagnetic fields by means of the mode matching method [4, 5].

## THEORETICAL BACKGROUND

In this section we will show the expressions for electromagnetic field decomposition in a closed volume. The derived equations are the basis for the mode matching method.

Given a volume $V$, enclosed in an ideal surface $S$, the scattered electromagnetic fields E and H may be decomposed by means of the Helmholtz theorem in summation of irrotational and solenoidal eigenmodes which constitute a complete set. We can write:

$$\bar{E} = \sum_n V_n \bar{e}_n + \sum_n F_n \bar{f}_n, \tag{1a}$$

$$\bar{H} = \sum_n I_n \bar{h}_n + \sum_n G_n \bar{g}_n, \tag{1b}$$

where $\bar{e}_n$ and $\bar{h}_n$ are orthonormal solenoidal eigenvectors and $\bar{f}_n$ and $\bar{g}_n$ irrotational ones. In Table 1 is listed a set of eigenvectors and the relative differential equations and boundary conditions they have to satisfy ($\bar{n}_o$ is the unit vector normal to $S$ pointing internally the volume) [5].

Table 1: Eigenvector equations

| Eigenvector | In volume $V$ | On surface $S$ |
|---|---|---|
| $\bar{e}_n$ | $\nabla \times \bar{e}_n = k_n \bar{h}_n$ | $\bar{n}_o \times \bar{e}_n = 0$ |
| $\bar{f}_n = \nabla \Phi_n$ | $\nabla^2 \Phi_n + \mu_n^2 \Phi_n = 0$ | $\Phi_n = 0$ |
| $\bar{h}_n$ | $\nabla \times \bar{h}_n = k_n \bar{e}_n$ | $\bar{n}_o \cdot \bar{h}_n = 0$ |
| $\bar{g}_n = \nabla \Psi_n$ | $\nabla^2 \Psi_n + \nu_n^2 \Psi_n = 0$ | $\partial \Psi_n / \partial n = 0$ |

Since the eigenvectors are determined by the geometry of the structure under study, the problem reduces in finding the coefficients $V_n, I_n, F_n, G_n$. This can be done by imposing the continuity of the em-field on the openings in the surface $S$. It is understood that in this matching one must take into account also the impressed field generated by the sources.

Because of the homogenous boundary condition, which is an intrinsic property of the eigenmodes, it is not possible to perform *tout court* the matching of the electric field.

This difficulty can be surmounted resorting to a procedure which will be described in the sequel.

Let be $\bar{\mathrm{E}}$ the given imposed electric field on the surface $S_0$ . Consider the quantity $\nabla \cdot (\bar{\mathrm{E}} \times \bar{h}_n^*)$ and resort to simple algebra to get the following expression:

$$\nabla \cdot (\bar{\mathrm{E}} \times \bar{h}_n^*) = \bar{h}_n^* \cdot (\nabla \times \bar{\mathrm{E}}) - \bar{\mathrm{E}} \cdot (\nabla \times \bar{h}_n^*)$$

Now into the RHS make use of Maxwell's equation for $\bar{\mathrm{E}}$ and the expression (1a), then integrate in the volume $V$. Applying the divergence theorem and exploiting the orthonormality of the eigenmodes, one may get the following expression:

$$\int_{S_o} (\bar{\mathrm{E}} \times \bar{h}_n^*) \cdot \bar{n}_o dS = -jkZ_o I_n - k_n V_n$$



ISBN 978-3-95450-118-2

where $S_o$ is the surface on which the electric field $\bar{\mathrm{E}}$ is impressed. Doing the same for the quantity $\nabla \cdot (\bar{e}_n^* \times \bar{\mathrm{H}})$ we have:

$$0 \equiv \oint_{S_o} (\bar{e}_n^* \times \bar{\mathrm{H}}) \cdot \bar{n}_o dS = k_n I_n - j\, kY_o V_n$$

From which we get the coefficients $I_n, V_n$:

$$I_n = \frac{jk\, Y_o}{(k^2 - k_n^2)} \int_{S_o} \left(\bar{\mathrm{E}} \times \bar{h}_n^*\right) \cdot \bar{n}_o dS \qquad (2a)$$

$$V_n = \frac{-j\, k_n\, Z_o}{k}\, I_n. \qquad (2b)$$

Analogously we may proceed for the irrotational fields, obtaining:

$$G_n = j \frac{Y_o}{k} \int_{S_o} (\bar{\mathrm{E}} \times \bar{g}_n^*) \cdot \bar{n}_o dS \qquad (3a)$$

$$F_n = 0. \qquad (3b)$$

The results of the above procedure may appear contradictory. We have imposed the use of the eigenmodes which satisfy homogeneous boundary conditions: one might be tempted to infer that the expansion coefficients should vanish. There is, indeed, no contradiction: the result on the LHS is obtained integrating on the volume $V$ a function definite positive, while the result at the RHS is obtained integrating on the surface $S_o$ the "imposed" field $\bar{\mathrm{E}}$. However, such an expansion will only behave non-uniformly convergent. This behaviour will impose some caution on the expansion truncation.

## IMPLEMENTATION OF THE METHOD

The structure we studied is shown in Figure 1: the regions I and II represent the cylindrical left and right beam pipes where the reflected fields will propagate $(z \in (-\infty, 0) \cup (L, +\infty), r \in (0, b))$, region III is the toroidal insert $(z \in (0, L), r \in (b, c))$ where radial waves can propagate, and region IV is the cavity where resonances can be excited $(z \in (0, L), r \in (0, b))$.

The beam $\rho_z(r, z; \omega)$ is represented in frequency domain as a thin ring of radius $a$ and charge $Q$ [1]:

$$\rho_z(r, z; \omega) = \frac{Q}{2\pi a} \delta(r - a) e^{-jk_0 z}, \qquad (4)$$

where $k_0 = \omega/\beta c$ is the propagation constant of the beam.

In order to handle the problem of determining the longitudinal beam coupling impedance, the electromagnetic field induced by the beam current will be calculated as a superposition of a source and a scattered field:

$$\bar{E}^{(tot)} = \bar{E}^{(source)} + \bar{E}^{(scattered)}$$

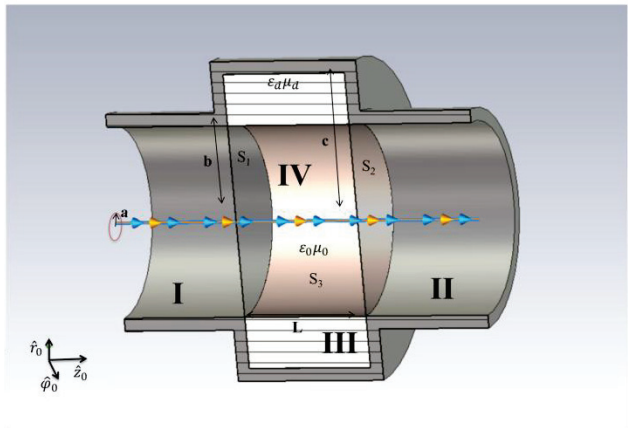


Figure 1: Model studied with the mode matching method.

The source field and the scattered field in all the four regions consist in Transverse Magnetic (TM) waves: all the components can be derived from the longitudinal electric field $E_z$.

### *Source Fields*

The source field $\bar{E}^{(source)}$ is calculated as the field induced by the source particle travelling at speed $\beta c$, i.e. representing a current $J_z = \rho_z \beta c$, along the axis of the perfectly conducting (PEC) beam pipe of radius $b$. This field is given by the following formula [1],

$$E_z^{(source)} = \frac{j\alpha_b Q\, Z_0}{2\pi\gamma^2 \beta b} \left[ K_0(u) - \frac{K_0(x)}{I_0(x)} I_0(u) \right] e^{-jk_0 z}, \qquad (5)$$

where $Z_0 = 376.73\Omega$ is the characteristic impedance of vacuum, $K_0, I_0$ the modified Bessel functions of argument $x = k_0 b/\gamma$ and $u = k_0\, r$.

### *Scattered field*

In region I we have the following expression for the longitudinal electric field [4, 5]:

$$E_z^{(left)} = \sum_p^{\infty} \boldsymbol{C_p} \frac{J_0(\alpha_p r/b)}{b\sqrt{\pi} J_1(\alpha_p)} e^{j\tilde{\alpha}_p z/b}. \qquad (6)$$

In region II we have

$$E_z^{(right)} = \sum_p^{\infty} \boldsymbol{D_p} \frac{J_0(\alpha_p r/b)}{b\sqrt{\pi} J_1(\alpha_p)} e^{-j\tilde{\alpha}_p (z-L)/b}, \qquad (7)$$

where $\alpha_p$, with $p \in \mathrm{N}$, are the zeros of the Bessel function $J_0(r)$, $\tilde{\alpha}_p = \sqrt{\alpha_0^2 - \alpha_p^2}$, $\alpha_0 = k_0 b = \omega\sqrt{\mu_0 \varepsilon_0}\, b$, $\alpha_1 = 2.405$.

In region III:

ISBN 978-3-95450-118-2

$$E_z^{(rad)} = \sum_s^{\infty} \boldsymbol{A_s}\, W_s(\hat{\alpha}_s r/b)cos(\alpha_s z/b), \qquad (5)$$

where the function $W_s(\tilde{\alpha}_s r/b)$ describe the radial waves as [4, 5]:

$$W_s(\hat{\alpha}_s/b) = H_0^{(2)}\left(\frac{\hat{\alpha}_s r}{b}\right) - \frac{H_0^{(2)}\left(\frac{\hat{\alpha}_s c}{b}\right)}{H_0^{(1)}\left(\frac{\hat{\alpha}_s c}{b}\right)} H_0^{(1)}\left(\frac{\hat{\alpha}_s r}{b}\right),$$

with $\alpha_d = k_d b = \omega\sqrt{\mu_d \varepsilon_d}\, b$, $\alpha_s = s\pi b/L$, where $d$ refers to the dielectric insert and $\hat{\alpha}_s = \sqrt{{\alpha_d}^2 - {\alpha_s}^2}$ and $Z_d$ is the characteristic impedance in this region.

In region IV we can expand the fields in the complete set of orthonormal modes of TM type associated to homogeneous boundary condition on $S_1$, $S_2$ and $S_3$:

$$\bar{E}^{(cav)} = \sum_{p,s} \boldsymbol{V_{ps}}\, \bar{e}_{ps}. \qquad (6)$$

The longitudinal component of the electric field has the following expression:

$$E_z^{(cav)} = \sum_{p,s}^{\infty} \boldsymbol{V_{ps}} \frac{\alpha_p}{\alpha_{ps}} \sqrt{\frac{\varepsilon_s}{L}} \frac{J_0\left(\frac{\alpha_p r}{b}\right)}{b\sqrt{\pi} J_1(\alpha_p)} cos\left(\frac{\alpha_s z}{b}\right), \qquad (7)$$

where $\alpha_{ps} = \sqrt{\alpha_p^2 + \alpha_s^2}$. It can be proved that the irrotational modes $\bar{g}_{ps}$ do not couple for the structure under study.

To summarize four infinite vectors $\{\boldsymbol{V_{ps}}\}$, $\{\boldsymbol{A_s}\}$, $\{\boldsymbol{C_p}\}$ and $\{\boldsymbol{D_p}\}$ are the unknowns.

### *Matching conditions*

By matching the tangential components of the magnetic field on the boundary surfaces $S_1$, $S_2$, $S_3$, we obtain 3 functional equations. By means of an ad-hoc projection (Ritz-Galerkin method [5]) each functional equation may be transformed into an infinite set of linear equations.

In order to get a fourth equation we should find a tool to match the tangential component of the electric field. This is not as simple as for the magnetic field since, according to the assumed expansion, the tangential component of the electric field on the boundary $S_0 = S_1 \cup S_2 \cup S_3$ is null by definition. Note that in the present case $S_0 \equiv S$. As previously mentioned, the expansion given by Eq. (7) will not converge uniformly on the boundaries. However, this difficulty may be circumvented by resorting to the equations (2a) and (2b):

$$\boldsymbol{V_{ps}} = \frac{\alpha_0 b}{(\alpha_0^2 - \alpha_{ps}^2)} \int_{S_0} \left(\bar{E} \times \bar{h}_{ps}^*\right) \cdot \hat{r}_0\, dS. \qquad (8)$$

An ad-hoc truncation is applied to the infinite set of the linear equations and then the four sets of equations are solved.

Once all the vectors are known, the coupling impedance can be easily calculated.

## APPLICATIONS

### *General tests*

A first series of benchmark was done with already developed theories and CST [6] particle simulations.

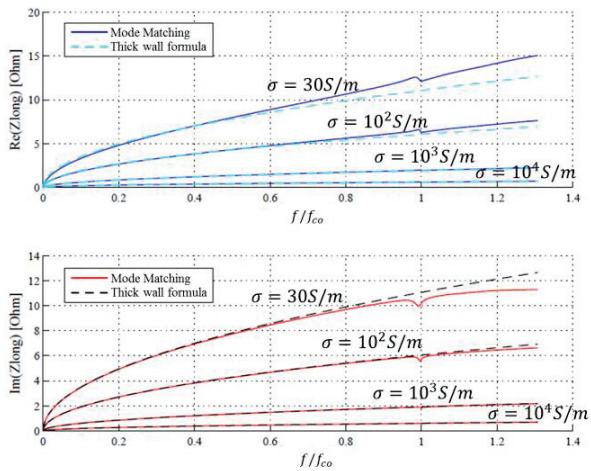


Figure 2: Comparison of the mode matching method (full lines) with the standard thick wall formula (dashed lines) for various conductivities and b=5cm, c=30cm, L=20cm; $\varepsilon_d = 8\varepsilon_0 - j\,\sigma/\omega$; $\mu_d = \mu_0$; $f_{co} = \alpha_1 c\,/2\pi b$.

In Figure 2 we show the comparison with the standard theory for thick wall [7]: the agreement is good for high conductivity, while it starts to be different for low conductivity at frequencies above cut-off ($f$ is normalized to the cut-off frequency $f_{co}$). In fact, with decreasing conductivity the insert surface impedance becomes more and more different from the surface impedance of the adjacent pipes I and II. This implies that the losses due to the scattered wave into the pipes, which can propagate only above cut-off, become comparable to those produced into the volume IV. As a conclusion, when a pipe exhibits a discontinuity in the surface impedance this discontinuity will contribute to increase the broad band impedance. This effect is not taken into account by the standard theory.

To complete the picture, in Figure 3 we study the impedance for different conductivities in comparison with Shobuda-Chin-Takata's model (S.C.T.) for resistive insert impedances [2]. The differences between the models are the absence of the outer PEC boundary layer and longitudinal modes. At the frequency in which the skin depth becomes comparable with the transverse dimension of the cavity, the two models start to differ: the transverse field can "see" the cavity's boundary and is reflected in our model, and radiated in the S.C.T. one. The longitudinal modes, in this case, do not play any



ISBN 978-3-95450-118-2

significant role, due to the high conductivity and the short longitudinal dimension.

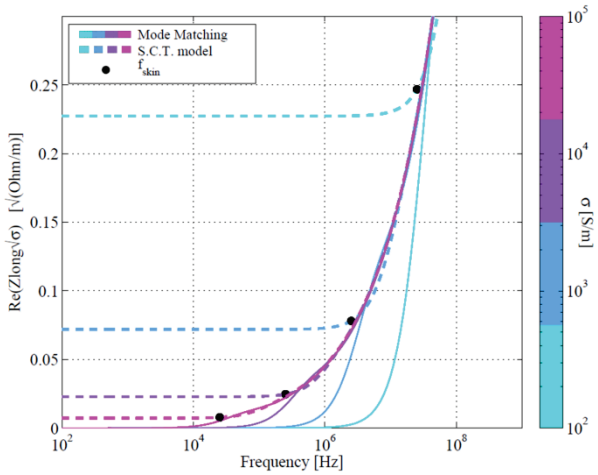


Figure 3: Comparison of Mode matching method with S.C.T. one.

In Figure 4 we show another comparison for a material with low conductivity ($\sigma \cong 10^{-2}\ S/m$): the cut-off between resonant modes and broadband behaviour is clearly visible. The discrepancy above cut-off is thought to be intrinsic to the CST solving tool.

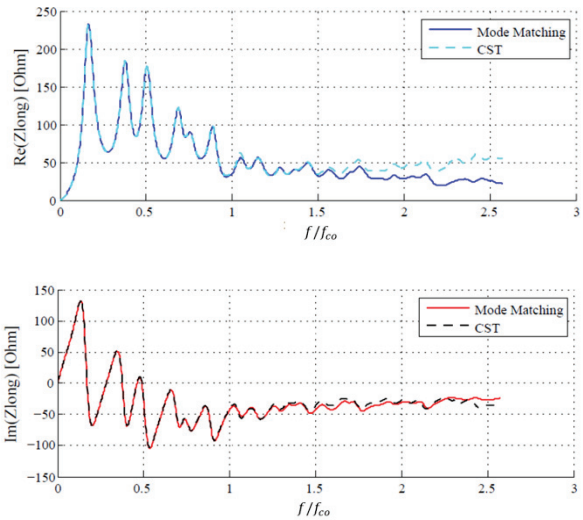


Figure 4: Comparison with CST simulations: b=5cm, c=30cm, L=20cm. Material: $\varepsilon_{dr}$=1, $\mu_{dr}$=1, $\sigma$=$10^{-2}$ S/m.

## *Application to an SPS enamel flange*

A cross-check was done in order to study the SPS flanges impedance. A flange can be seen as a very short re-entrance between two beam pipes whose impedance cannot be easily studied with CST due to geometrical limitations (800 μm gap width with 5 cm beam pipe radius) and due to the very low dielectric losses that make the Q factor - and then the wake length - very large.

Figure 5 shows the comparison between the Mode Matching and CST for the first impedance peak at 660 MHz. The three smaller plots show the convergence accuracy for the three fit parameters: quality factor $Q$, shunt impedance $R_s$, resonance frequency $f_{res}$. In CST, the impedance was scanned in function of the wake length and mesh cells to maximum values of 60m and 600k meshes before memory saturation, in mode matching in function of longitudinal $S$ and radial modes $P$, to a maximum of 15 and 50 modes. The values all agree within less than 1%.

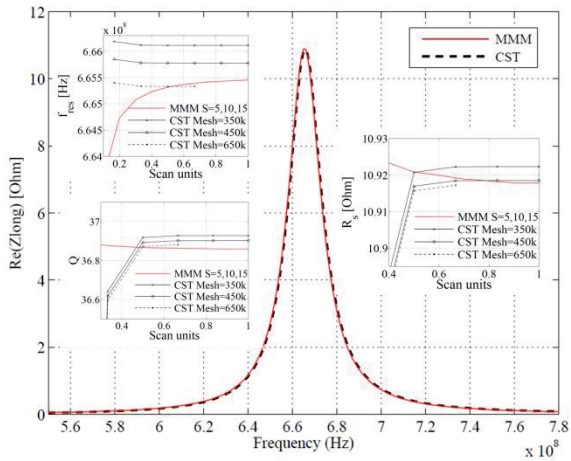


Figure 5: Comparison with CST simulations: b=5cm, c=9cm, L=800um. Material: $\varepsilon_{dr}$=9.9, $\mu_{dr}$=1, $\sigma$=$10^{-2}$ S/m. Peak resonance at 664 MHz with convergence tests of quality factor $Q$, shunt impedance $R_s$, resonance frequency $f_{res}$ in the smaller plots. The horizontal axis "Scan units" refers to P/max(P) for Mode Matching and Wake length/ max(Wake length) for CST.

## *Application to non-ultrarelativistic cases*

In the following we present some studies on non ultrarelativistic beams, for different kinds of filling materials.

In Figure 6 it is shown the beta dependence of longitudinal impedance in case of copper as filling material: all curves are below the relativistic case. It is worth to notice that the impedance is changing considerably from roughly 10MHz.

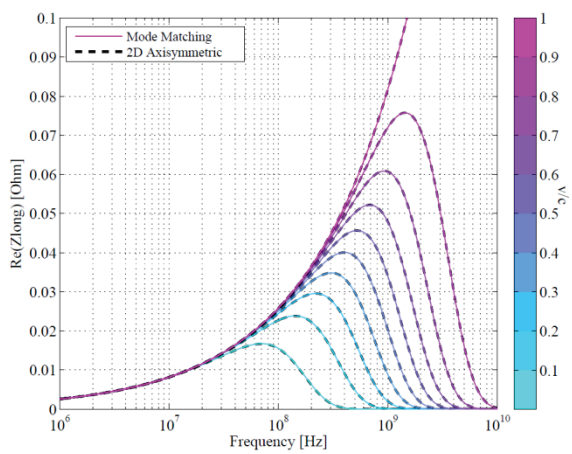


Figure 6: Resistive wall impedance for different β.

ISBN 978-3-95450-118-2

Impedance decreases accordingly with beam field decaying. b=5cm, c=30cm, L=20cm. Material: $\varepsilon_{dr}$=1, $\mu_{dr}$=1, $\sigma$=5.98 $10^6$ S/m

Since, in this particular problem, it can be shown that the only driving term playing a role in the matching equations is $H_\varphi$, it is expected that the impedance decreases with β accordingly to $H_\varphi$ as shown in Figure 7. The method was benchmarked with a 2D axisymmetric code developed at CERN by N.Mounet et al. [8].

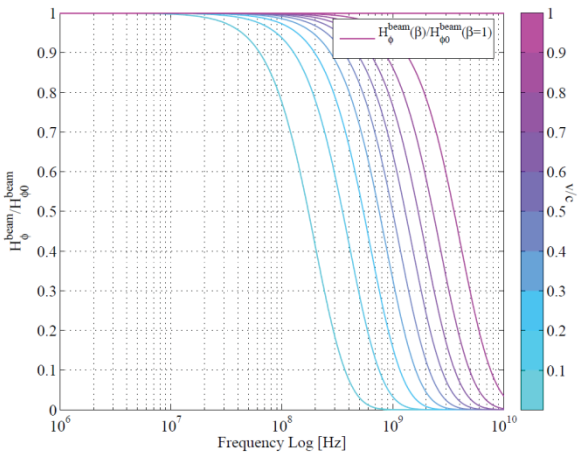


Figure 7: Azimuthal component of the source magnetic field $H_\varphi$ in function of β. For the lowest case ($\beta = 0.1$) the field is half the ultrarelativistic one around 10MHz.

Confirmation of this behaviour and of the reliability of the code is given in Figure 8, where the case of a dispersive material (Ferrite 4A4) is displayed. The impedance is not changing significantly below 10 MHz.

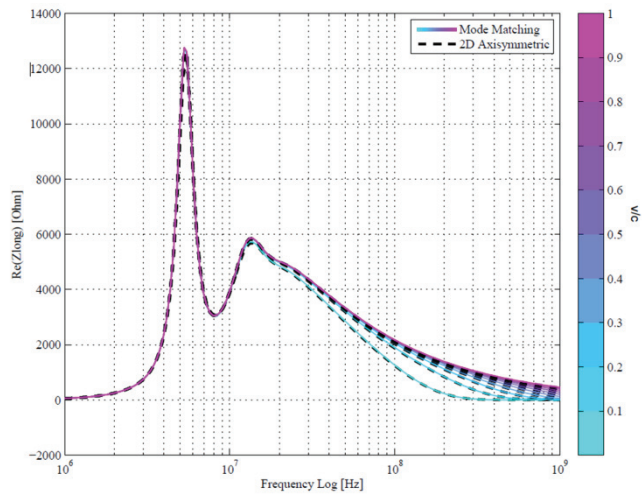


Figure 8: Impedance from a ferrite load varying β. b=5cm, c=30cm, L=20cm. Material: $\varepsilon_{dr}$=12, $\mu_{dr}$=1+460/(1+jf/20e6), $\sigma$=$10^{-6}$ S/m.

The case of the thin insert has been also analysed in function of β. In Table 2 the three parameters $f_{res}$, $Q$, and $R_s$ together with the power loss and the magnetic stored energy calculated in the region III with Poynting theorem [4, 5] are reported. As expected, the $Q$ value is not changing with β (it depends on the material properties) as the $f_{res}$ (depends on geometry). What changes is $R_s$ depending on the excitation source. Being above 10MHz the impedance is decreasing with β accordingly to $R_s$.

Table 2: Resonance parameters in function of β for thin alumina insert.

| $\beta$ | $f_{res}$ [Hz] | $R_s$ [Ω] | $Q$ | $W_m$ [J] | $P_l$ [W] |
|---|---|---|---|---|---|
| 1 | 6.65E+08 | 10.94 | 36.90 | 1.27E-08 | 1.45 |
| 0.8 | 6.65E+08 | 9.56 | 36.90 | 1.11E-08 | 1.27 |
| 0.6 | 6.65E+08 | 7.26 | 36.88 | 8.45E-09 | 0.97 |
| 0.4 | 6.64E+08 | 3.59 | 36.83 | 4.18E-09 | 0.48 |
| 0.2 | 6.64E+08 | 0.24 | 36.51 | 2.73E-10 | 0.03 |

## CONCLUSION

The longitudinal beam coupling impedance of a finite length device was successfully derived and benchmarked with existing theory and numerical simulations also in the non ultrarelativistic case.

Considering the real finite length of a device is important both for high conductivity materials, and for low conductivity ones: in the first case the impedance above cut-off has to include the contribution of the beam pipes; in the second case the resonances depend on the length of the device and the losses in the material, this could lead to beam coupling instability if these modes are not properly damped (lowering the Q factor).

The study of impedance as a function of relativistic β showed the reliability of the code in comparison with the existing 2D azimuthal code for various cases. For this particular geometry, the impedance decreases with β accordingly to the decay of the driving fields above roughly 10MHz.

Further extension to the driving (dipolar) and detuning (quadrupolar) impedances is under development.

## REFERENCES

[1] R.L Gluckstern, B.Zotter, "Longitudinal Impedance of a Resistive Tube of Finite Length", CERN unpublished.
[2] Y. Shobuda, Y.H. Chin, K. Takata "Coupling impedances of a resistive insert in a vacuum chamber", PhysRevSTAB, 2009.
[3] G. Stupakov, " Resistive wall impedance of an insert", SLAC-PUB-11052 – 2005.
[4] G. Franceschetti, "Electromagnetics: Theory, Techniques, and Engineering Paradigms " Springer-Verlag New York, June 1997.
[5] J. G. Van Bladel, "Electromagnetic Fields",(IEEE Press Series on Electromagnetic Wave Theory, 2007.
[6] CST Computer Simulation Technology AG.
[7] L. Palumbo, V.G. Vaccaro, M. Zobov, "Wake Fields and Impedance", CAS school 1994.
[8] N.Mounet, E. Métral, "Impedances of an Infinitely Long and Axisymmetric Multilayer Beam Pipe: Matrix Formalism and Multimode Analysis", IPAC 2010.



ISBN 978-3-95450-118-2